Processing parameters investigation for the fabrication of self-supported and freeform polymeric microstructures using ultraviolet-assisted three-dimensional printing

2014 J. Micromech. Microeng. 24 055020

(http://iopscience.iop.org/0960-1317/24/5/055020)

IOP Publishing Journal of Micromechanics and Microengineering
J. Micromech. Microeng. **24** (2014) 055020 (12pp) doi:10.1088/0960-1317/24/5/055020

Processing parameters investigation for the fabrication of self-supported and freeform polymeric microstructures using ultraviolet-assisted three-dimensional printing

R D Farahani, L L Lebel and D Therriault

Laboratory for Multiscale Mechanics, Center for Applied Research on Polymers (CREPEC), École Polytechnique de Montréal CP 6079, succ Centre-Ville, Montreal, H3C 3A7, Canada

E-mail: daniel.therriault@polymtl.ca

Received 13 December 2013, revised 18 March 2014
Accepted for publication 19 March 2014
Published 15 April 2014

Abstract

Ultraviolet-assisted three-dimensional (3D) printing (UV-3DP) was used to manufacture photopolymer-based microdevices with 3D self-supported and freeform features. The UV-3DP technique consists of the robotized deposition of extruded filaments, which are rapidly photopolymerized under UV illumination during the deposition process. This paper systematically studies the processing parameters of the UV-3DP technique using two photo-curable polymers and their associated nanocomposite materials. The main processing parameters including materials' rheological behavior, deposition speed and extrusion pressure, and UV illumination conditions were thoroughly investigated. A processing map was then defined in order to help choosing the proper parameters for the UV-3DP of microstructures with various geometries. Compared to self-supported features, the accurate fabrication of 3D freeform structures was found to take place in a narrower processing region since a higher rigidity of the extruded filament was required for structural stability. Finally, various 3D self-supported and freeform microstructures with high potential in micro electromechanical systems, micro-systems and organic electronics were fabricated to show the capability of the technique.

Keywords: UV-assisted 3D printing, microstructures, 3D freeform, UV-curable polymers, processing map

(Some figures may appear in colour only in the online journal)

1. Introduction

Micro- and nanotechnological systems using photopolymers and their associated nanocomposite materials have gained considerable attention in various fields such as micro electromechanical systems (MEMS) [1], microelectronics [2], optoelectronics [3], biotechnology [4] and microchemical systems [5]. Despite the wide variety of applications, device miniaturization and three-dimensional (3D) shape optimization have not reached their full potential, partly because of the lack of easy and cost-effective manufacturing techniques. Standard microfabrication techniques such as stereolithographic techniques [6, 7] have been adapted to fabricate 3D products using photopolymers. Ultraviolet-assisted 3D-printing (UV-3DP) [8] is an alternative technique to manufacture photopolymer-based microdevices with 3D freeform or supported features. Figure 1 is a schematic of the UV-3DP fabrication of a freeform helical microspring.

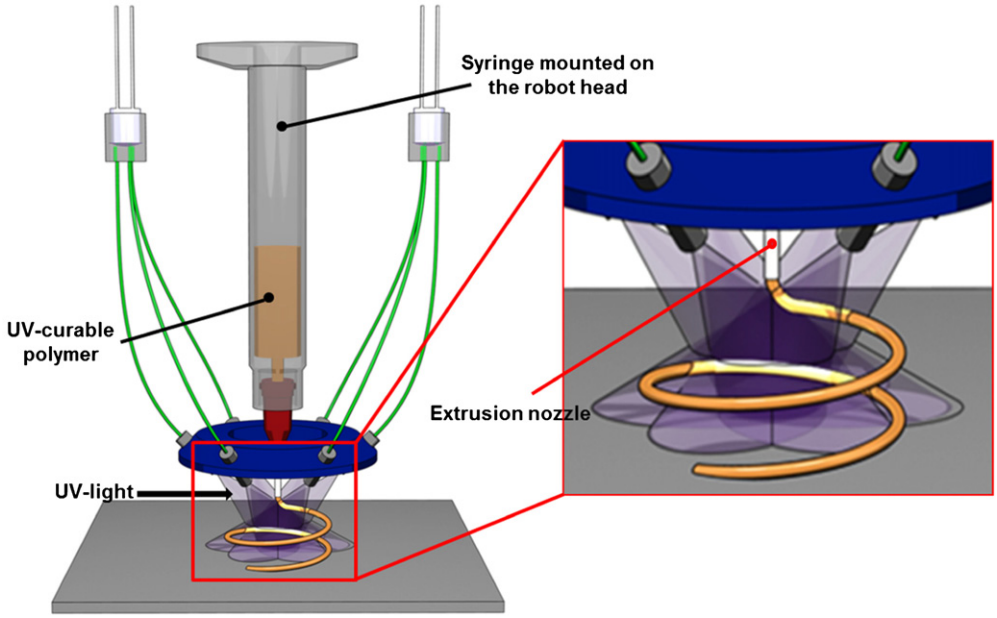

Figure 1. A scheme of the UV-assisted fabrication of a microspring made of a photopolymer. The material is extruded through a micronozzle and rapidly photopolymerized under the UV illumination provided by a set of optical fibers.

This technique relies on the robotically-controlled micro-extrusion of a UV-curable ink filament through a capillary nozzle while the extrusion point is moved in three directions. The uncured ink material is photopolymerized within seconds after extrusion under UV illumination that moves along the extrusion point. Upon curing, the increased rigidity of the extruded filament enables the creation of multi-directional shapes (3D freeform and self-supported) layout along the trajectory of the extrusion point. Compared to conventional microfabrication techniques, the UV-3DP exhibits a high level of flexibility, cost-effectiveness and fabrication rate.

Despite the flexibility of the UV-3DP technique, the type of UV-curable materials as well as the processing parameters have to be carefully adjusted to build a precise 3D microstructure. In this paper, we systematically investigate all the main processing parameters such as deposition speed (i.e., velocity of the micronozzle motion relative to the substrate), extrusion pressure, material viscosity, and UV-exposure region. The influence of each parameter was studied for the fabrication of 3D self-supported and freeform microstructures using the UV-3DP of UV-curable thermosetting resins and their associated nanocomposite materials. One of the main outcomes of this investigation is the creation of a processing map which can be used as a guide for the fabrication of different 3D geometries.

2. Experimental details

2.1. Materials

The materials used as the ink materials in this study were commercially available one-component dual cure schedule (UV/heat curable) resins which were used either as they were received or after being rheologically modified (e.g., mixing with nanoparticles). The resins were either polyurethane-based (NEA123MB & NEA123T, Norland Products) or epoxy-based (UV15DC80, Master Bond Inc.) materials. The resins contained UV photo-initiators having a maximum absorption at 365 nm and a heat-initiator active in the 60–80 °C range. Nanoparticles such as fumed silica (Aerosil 200, Degussa) and single-walled carbon nanotubes [9] were added to the resins to make nanocomposite inks. These nanocomposite ink materials were prepared by blending the resins and the nanofillers using ultrasonication and three-roll mill mixing methods (more details on the nanocomposite inks preparation can be found elsewhere [8–10]). The inks were stored in UV-protective 3CC syringes (Nordson EFD) at room temperature. Based on our experience, the materials remain stable at least for a year under the above conditions.

2.2. UV-3DP experimental setup

Figure 2 shows images of the UV-3DP set-up and deposition of a microspring using this technique. The UV direct-writing platform is composed of a computer-controlled robot (I & J2200-4, I & J Fisnar) that moves a dispensing apparatus (HP-7X, EFD) and a UV light-emission set-up along the x, y and z axes using a commercial software (JR Points for Dispensing, Janome Sewing Machine). The dispensing apparatus mounted on the robot head carries a 3 CC syringe (Nordson EFD) containing the ink material (figure 2(a)) which is then extruded by an applied pressure. This apparatus is connected to a pneumatic fluid dispenser (Ultra^{TM} 2400 series, EFD) which can provide an extrusion pressure up to 4.9 MPa. The UV light is provided by two high-intensity UV light-emitting diodes (NCSU033A, Nichia) having a wavelength centered at 365. A set of six optical fibers arranged in a circular pattern (figure 2(c)) deliver the UV light close to the tip of the extrusion micronozzle (Precision Stainless Steel Tips, EFD). The intensity of the present UV radiation is

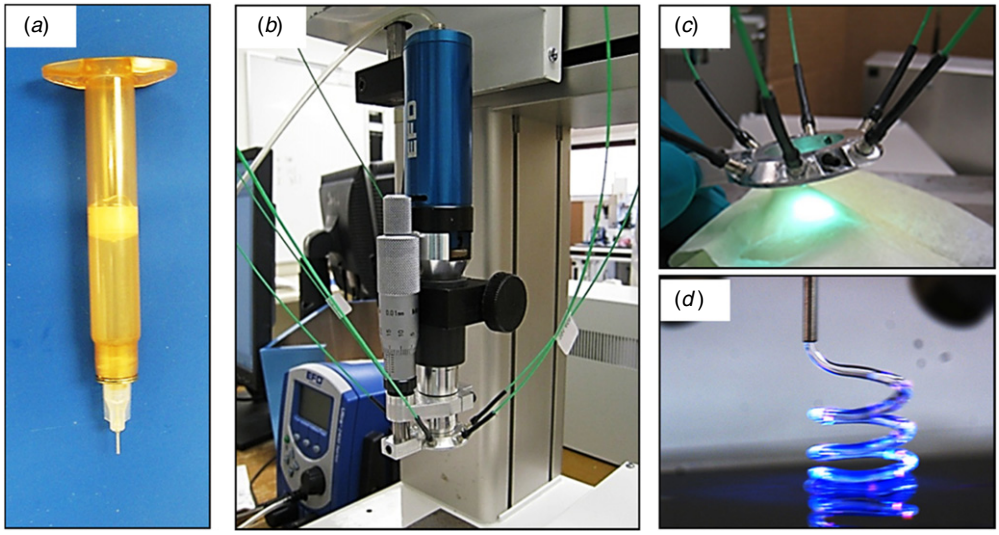

Figure 2. (*a*) a 3 CC syringe containing a UV-curable material, (*b*) the deposition set-up with inserted syringe and pressure piston, mounted on the computer-controlled robot, (*c*) UV light delivery system consisting of six fiber optics showing UV radiation emitted (mounted on the robot in (*b*)), and (*d*) image of a microspring deposition using a UV-curable ink.

50 mW cm^{-2} measured using a UV intensity probe (UV Intensity meter, model 100, Karl Suss) [8]. The fast-curing of the ink enables the fabrication of self-supported and freeform 3D structures when the extrusion position spatially changes (figure 2(*d*)).

2.3. UV-3DP Fabrication of 3D self-supported and freeform microstructures

Stainless steel micronozzles with two different internal diameters (ID of 100 and 150 μm) were used with 3 CC syringes. As a self-supported structure, a 3D periodic scaffold was fabricated which has potential applications in tissue engineering [11]. The fabrication of the scaffold began with the deposition of the inks filaments on a substrate, leading to a 2D pattern. The following layers were deposited by successively incrementing the z-position of the dispensing nozzle by the diameter of the filaments and changing the dispensing direction by 90° rotation from the underlying layer. The fabricated scaffolds consisted of several layers (e.g., four layers) of the ink filaments, in which each layer was alternatively oriented perpendicular to or along the first deposited layer. This process was repeated until the desired 3D scaffold was created.

3D freeform microstructures featuring different geometries were also manufactured using the UV-3DP technique. The first fabricated microdevice was composed of a set of 16 freeform vertical filaments having a diameter of ~150 μm in a square layout of 4 × 4 microrods. Networks of 3D helical microstructures composed of up to 15 microsprings were also accurately manufactured.

2.4. Inks viscosity characterization

An experimental method based on capillary viscometry [10, 12] was used to estimate the process-related apparent viscosity of the inks. To obtain different shear conditions, ten continuous filaments of material were extruded through a micronozzle (5130-0.25-B, Precision Stainless Steel Tips, EFD, length of ~16 mm and internal diameter of 150 μm) at same pressure over a glass substrate and was repeated for five different pressures (i.e., 0.7, 1.4, 2.1, 2.8, and 3.5 MPa). The filaments were deposited using the dispensing robot with a calibrated deposition speed. Shortly after the deposition, the filaments were cured under a UV lamp (RK-97600, Cole-Parmer) illumination for 5 min. The material flow rate during the extrusion was calculated by multiplying the deposition speed by the deposited filaments cross-section. The cross-section area of the filaments was measured with an optical microscope (BX-61, Olympus) and image analysis software (Image-Pro Plus V6, Media Cybernetics). The possible error for the calculation of filament cross-section area upon curing was negligible since the materials shrinkage is <1% according to the supplier. The process-related apparent viscosity and the process-related shear rate were calculated from capillary viscometry equations including Rabinowitsch's correction [10, 12]. The end effects called Bagley correction were negligible in the viscosity calculations because of the very high capillary aspect ratio (i.e., length/diameter of the extrusion nozzle used: L/D ~ 106).

2.5. Morphological characterization of fabricated microstructures

The structures fabricated through different processing conditions were observed using an optical microscope (BX-61, Olympus) and image analysis software (Image-Pro Plus V7, Media Cybernetics) in order to find the processing map for a successful UV direct-writing. The morphology of the representative self-supported and freeform microstructures was also observed either by optical microscopy or field emission scanning electron microscopy (FESEM JEOL, JSM-7600TFE).

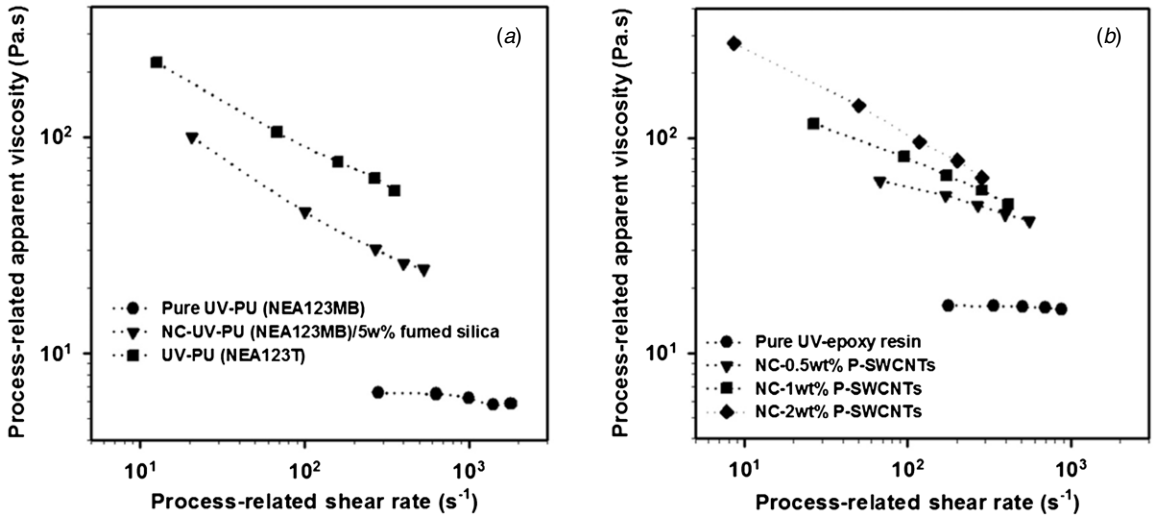

Figure 3. Process-related apparent viscosity of the ink materials with respect to process-related shear rate using a method based on capillary viscometry: (*a*) UV-curable urethane-based (UV-PU) resins and (*b*) UV-curable epoxy-based resin and its associated CNT-reinforced nanocomposites.

3. Results and discussion

3.1. Material properties

The materials viscosity is probably the most important parameter of the direct-write techniques. Materials with moderate to high viscosities are necessary to extrude stable filaments [13, 14]. Since the high viscosity may limit flow through fine extrusion nozzles, an extruded material shear-thinning behavior (i.e., a decrease of viscosity with an increase of shear forces inside the nozzle) is preferable. For shear-thinning inks, their rigidity increases when exiting the extrusion nozzle, that is, when the shear strain applied to the material returns to a near zero value. This rigidity allows the filaments shape retention and enables to fabricate self-supported 3D structures. However to fabricate freeform 3D structures, a further increase of rigidity is required that is provided by the polymerization of the inks in the UV-3DP technique [8].

Figure 3 shows the process-related apparent viscosity (η_{app}) with respect to the process-related shear rates ($\dot{\gamma}$) obtained using our capillary viscometry technique for all the materials used in this study. Figure 3(*a*) shows the viscometry results for the UV-curable urethane-based (UV-PU) materials. A nearly constant η_{app} of $\sim$ 6 Pa.s was observed for the pure NEA123MB, indicating a Newtonian behavior in the range of shear rates studied. The incorporation of 5 wt% silica nanoparticles into this pure resin resulted in a considerable increase (by 17-fold) for η_{app} at low $\dot{\gamma}$ and also a shear-thinning rheological behavior. This increase might be due to a weak network formation of hydrogen bonded fumed silica particles which caused a gel-like rheological behavior to the mixture at rest. The weakly bounded network is then destroyed under moderate shear force resulting in the reduction of the viscosity. The second type of UV-PU (NEA 123T) which was used as received (contains nanoparticles which were already added by the supplier) shows a relatively high viscosity and a shear-thinning behavior without further adding nanofillers (figure 3(*a*)). Figure 3(*b*) shows the results obtained for the viscosity of UV-curable epoxy-based (UV-epoxy) materials. Similar to the pure NEA123MB, a Newtonian behavior was observed for the viscosity of the UV-epoxy resin with a slightly higher value of $\sim$17 Pa.s. The η_{app} of the resin increased by the addition of 0.5 wt% of CNTs. Further increases of the viscosity were achieved with the increase of CNTs concentrations (1 and 2 wt%). A shear-thinning behavior of the resulting nanocomposites with different power-law indices (slope of the curves) was also observed. The carbon nanotubes high aspect ratio which possibly enabled the formation of a rheological percolation network and also their possible orientation during extrusion are thought to be responsible for the observed shear-thinning behavior.

Figure 4 shows the effect of viscosity (or rheological behavior) of three representative materials used in this study on the UV-3DP fabrication of freeform microsprings. Figure 4(*a*) shows an unsuccessful fabrication of the designed microspring when the low-viscosity Newtonian UV-PU (pure NEA123MB) was used. As it can been seen in the inset of figure 4(*a*), the viscosity of the material used seems not to be high enough to create a stable filament. Similar behavior was also observed for the low-viscosity Newtonian pure UV-epoxy (the result is not shown). However, the fabrication of microsprings was successful when the materials with higher viscosities were used. Figure 4(*b*) shows a representative optical image of a fabricated microspring with seven coils using the UV-PU (NEA 123T) and a stable filament is observed in the inset image. Similarly, a microspring with six coils was fabricated using the UV-epoxy containing 1 wt% CNTs as a result of its relatively high viscosity, as shown in figure 4(*c*). The higher viscosity prevents sagging of the extruded filament prior to curing under UV exposure, as a filamentary shape is observed for both materials in the inset of the figures.

In case of the pure low-viscosity resins, the addition of nanofillers was a key in order to increase the resins viscosity and make them suitable for a successful UV-3DP while

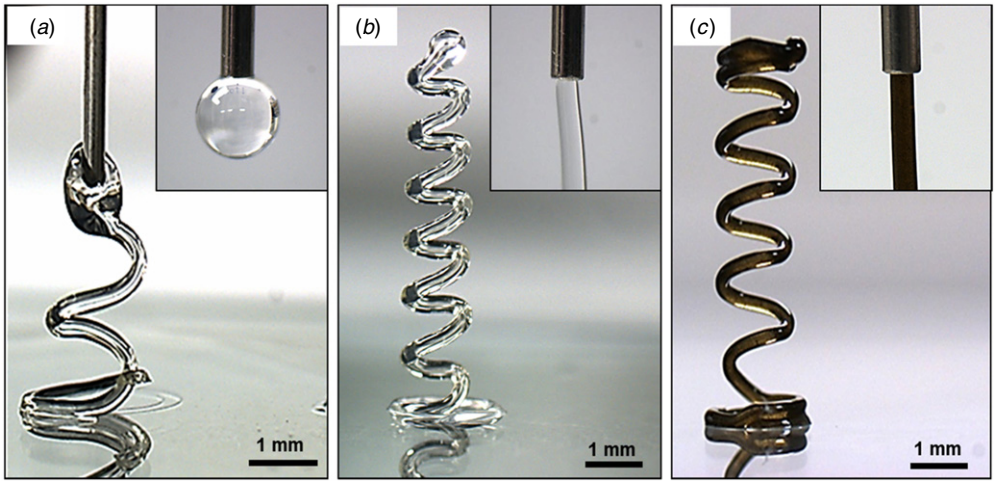

Figure 4. Optical images of UV-3DP fabrication of microsprings using three representative materials (*a*) the pure NEA123MB (low viscos material), and (*b*) and (*c*) NEA 123T and the UV-epoxy containing 1wt% CNTs (high viscosity materials). The images show the viscosity-dependent stability of filaments to build a structure with desired shape, in this case, a microspring.

the observed shear-thinning behavior facilitated materials extrusion at lower pressures. However, the addition of higher loadings, especially in case of CNTs may decrease the resins transparency and consequently their photopolymerization rates, and thus, lowers the fabrication rate.

3.2. Processing criteria

Material conversion rate, defined here as α which is the degree of materials solidification (i.e., 0 for the uncured viscous liquid to 100% for the completely cured solid) is a crucial parameter for an accurate UV-3DP. α depends on both the intrinsic properties of the material (e.g., type of monomer, photopolymerization mechanism, etc) and also processing-related parameters such as the thickness (or diameter) of the extruded filaments, the intensity of the UV source, its distance from the extrusion point and the UV exposure time. For an accurate 3D supported or freeform fabrication, the photoinitiated polymerization of monomers should occur within seconds to give a critical degree of materials conversion, defined here as α_c which is the required increase of rigidity. Figure 5 schematically represents the material-process-related photopolymerization mechanism during the UV-3DP fabrication of a filament. Depending on designed geometries, either self-supported or freeform features, a specific value for α_c may be required. In particular, to accurately fabricate a 3D freeform microspring, the extruded filament must stay under the UV-exposure for a certain time until it reaches enough rigidity, being able to mechanically support newly, yet liquid extruded material (high α_c values). This value may be lower for self-supported periodic scaffold or even for the vertical rods. Considering all the parameters, we can come to the conclusion that α_c is influenced by three major processing parameters: radiation exposure length (region), deposition speed and extrusion pressure, which are thoroughly discussed in the following sections. For each parameter, only representative optical images of structures fabricated using an extrusion nozzle of 150 μm-internal diameter and the UV-PU resin, NEA 123T will be shown. Finally, a processing map will be drawn to show the capability of the UV-3DP technique for the fabrication of various microstructures with different geometries.

3.2.1. Radiation exposure length (UV-exposure zone). The radiation exposure length or UV-exposure zone is shown in figure 5. This parameter is controlled by moving the UV source (i.e., the ring with six fiber optics shown in figure 2(*c*)) upward and downward. The UV-exposure zone is adjusted such that the filament is exposed to the UV radiation slightly after extrusion (i.e., extrusion to exposition length as shown in figure 5). This allows the increase in rigidity upon curing to occur away from the extrusion point. However, the UV radiation must nonetheless remain as close as possible to the extrusion point in order to reproduce the specific path of the moving extrusion device (i.e., short extrusion to exposition length as shown in figure 5).

Figure 6 shows the effect of radiation exposure length on the fabrication of freeform microsprings. Figure 6(*a*) is schematic of a designed microspring (five coils, coil diameter of 1 mm and filament diameter of 150 μm) to be fabricated while figures 6(*b*) and (*c*) show optical images of an unsuccessful fabrication resulting from an incorrect positioning of UV radiation apparatus. The material used here was UV-PU (NEA 123T) and the extrusion nozzle ID was 150 μm. Figure 6(*b*) shows the structures fabricated when the tip of extrusion nozzle met the UV-light (i.e., extrusion to exposition length equals to 0 mm) by which the nozzle might be clogged by the cured materials. However, when UV radiation was adjusted far from the extrusion nozzle (i.e., long extrusion to exposition length), the extruded filaments did not reach the desired rigidity (i.e., $\alpha < \alpha_c$) to provide structural support for the material being deposited, resulting in a non-shape structures (figure 6(*c*)).

3.2.2. Deposition speed. Figure 7 shows optical images of the vertical lines (figure 7(*a*)) and microsprings (figure 7(*b*)) fabricated at different deposition speed (0.1–0.7 mm s^{-1}) while

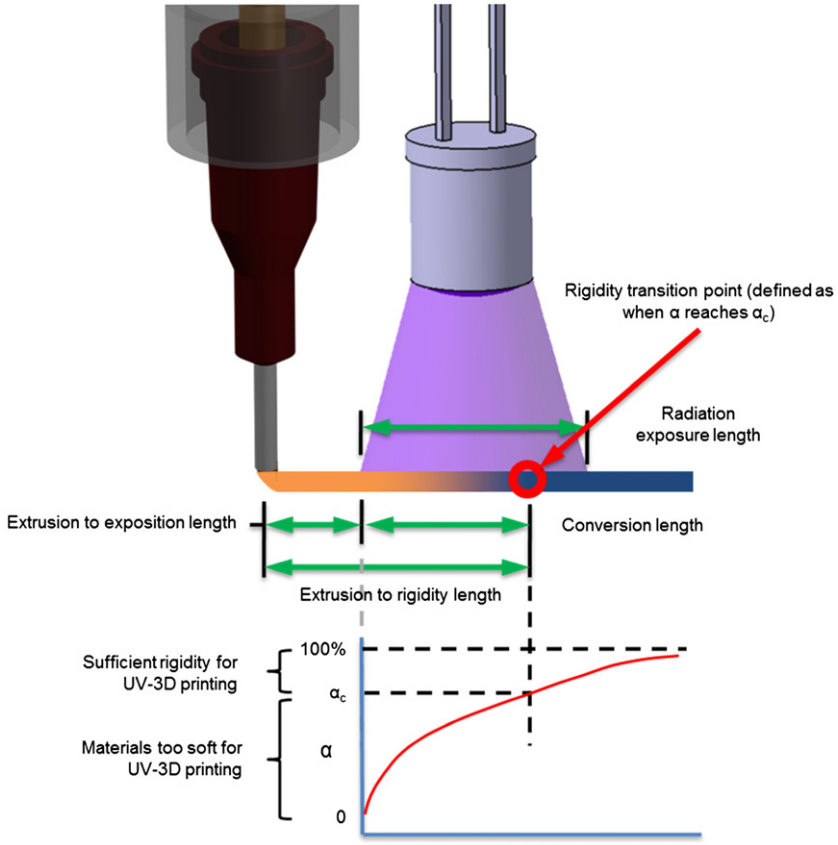

Figure 5. Schematic representation of the material-process-related photopolymerization mechanism during the UV-3DP fabrication of a filament.

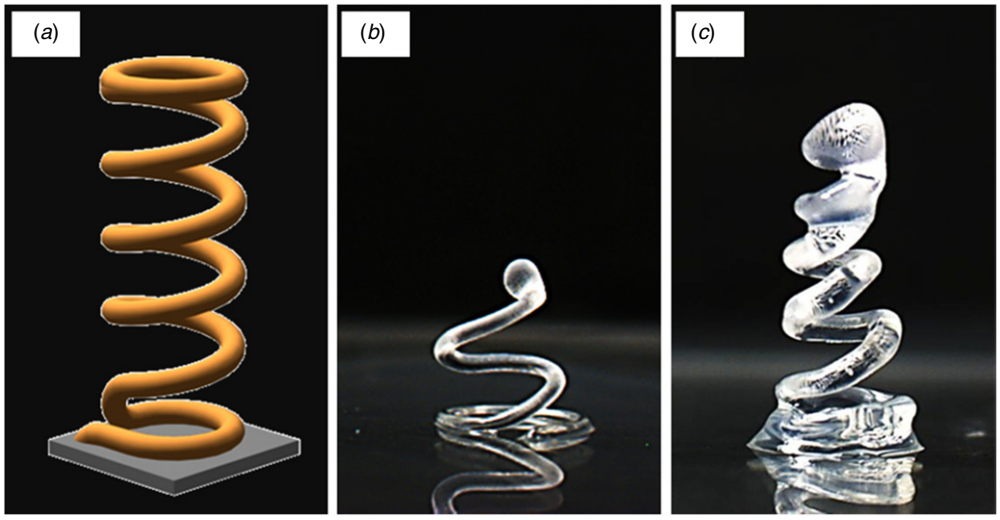

Figure 6. Incorrect adjustment of UV-exposure region: (*a*) virtual image of the programmed path of the extrusion nozzle, (*b*) the extrusion nozzle is very close to UV-exposure region, and (*c*) the extrusion nozzle is too far from UV-exposure region so the filament meets the UV light later than it has to. The deposition carried out at a deposition speed of 0.3 mm s^{-1} and extrusion pressure of ∼1 MPa using an extrusion nozzle of 150 μm-internal diameter and the UV-PU resin, NEA 123T.

maintaining a constant extrusion pressure of ∼1 MPa. In order to better interpret the results, the extrusion speed of the material inside the micronozzle was estimated for the extrusion pressure of ∼1 MPa. The extrusion speed cannot be controlled directly and is the extrusion pressure dependent. At the extrusion pressure of 1 MPa, the apparent viscosity of material was extrapolated from the viscosity curve of UV-PU (NEA 123T) shown in figure 3(*a*). The associated extrusion speed, $\bar{V}_E$, was then estimated from the following popular capillary equation:

$$\bar{V}_E = \frac{R^2 \Delta P}{8 \eta_{\text{app}} L} \tag{1}$$

where η_{app} is the extrapolated apparent viscosity of the material and ΔP is the pressure drop. R and L are radius and length of

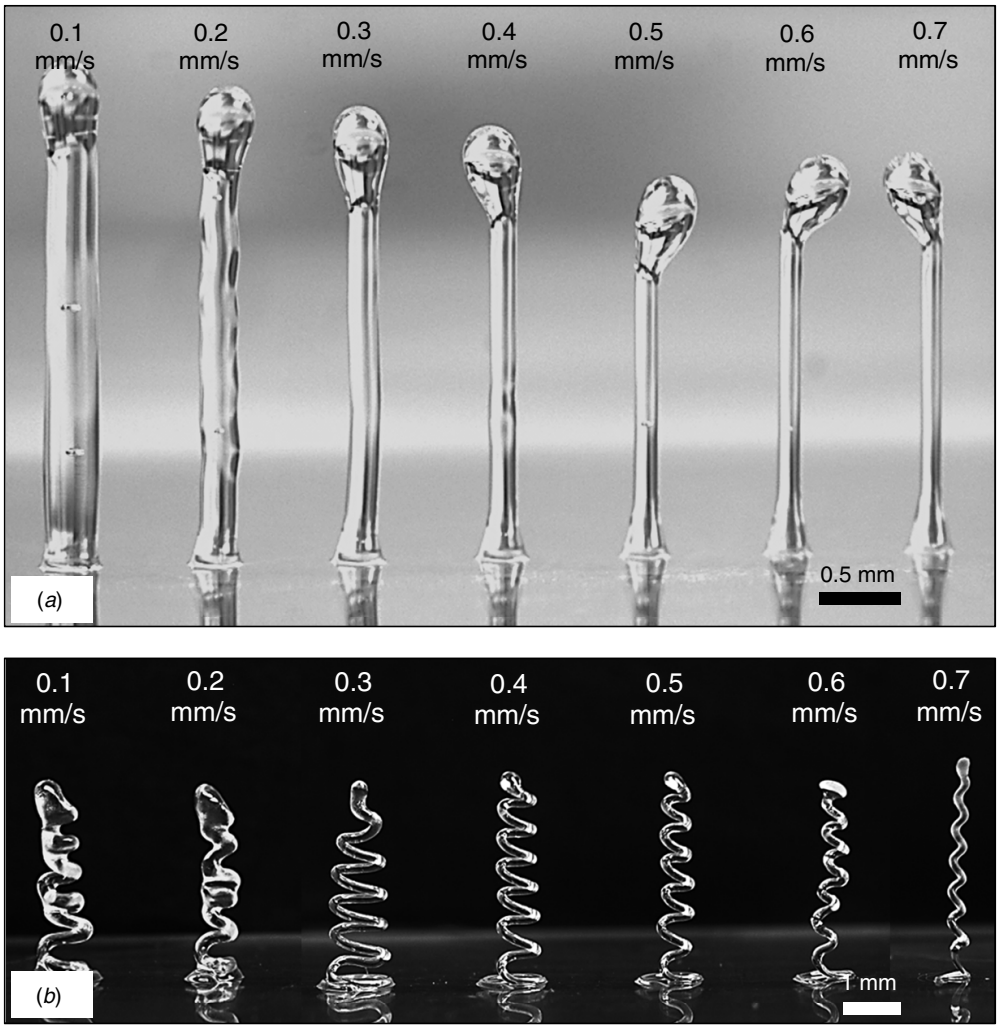

Figure 7. UV-3DP fabrication of (*a*) vertical filaments and (*b*) freeform microsprings at different deposition speeds and a constant extrusion pressure of ∼1 MPa using an extrusion nozzle of 150 μm-internal diameter and the UV-PU resin, NEA 123T.

the extrusion nozzle, respectively. It should be mentioned that the estimated extrusion speed value might not be accurate and was calculated to help better interpretation of the results by comparing the deposition and extrusion speeds. For the extrusion pressure of 1 MPa, the extrapolated value of the η was ∼115 Pa.s and the extrusion speed was estimated ∼0.4 mm s^{-1}. At the relatively low deposition speeds (0.1–0.2 mm s^{-1}), the lines were straight and stable having a diameter much larger than the internal needle diameter due to both mismatching the deposition speed (<0.4 mm s^{-1}) and the extrusion pressure/speed and also swelling of the material after the exit of the extrusion nozzle. The UV-exposure time was enough to allow the complete curing of the filaments (i.e., $\alpha \geqslant \alpha_c$) and thus, the fabricated lines were straight. However, a slight instability like waviness of the filaments was observed at the speed of 0.3 mm s^{-1}. The filaments' diameter varied depending on the material possible swelling and the deposition speed. As the deposition speed increased, the filaments diameter decreased and the straight filaments were observed. At the deposition speed of 0.4 mm s^{-1}, the filament was straight with a diameter close to the ID of the micronozzle, indicating the possible match between the deposition speed and extrusion pressure/speed. At higher speeds (0.6–0.7 mm s^{-1}), the possible stretching of the extruded material (deposition speed > extrusion speed) may also affect the filament diameter. As the deposition speed increased, the length of the vertical filaments reduced and a bubble-shape was observed at the top end of the vertical filament. The reason is that the extrusion nozzle moved to the robot origin after it reached the final extrusion point and thus the latest extruded materials did not meet the UV light enough to reach the required rigidity. Therefore, the short UV-exposure time (long extrusion to rigidity length) resulted in an incomplete polymerization of materials at the top of filaments (i.e., $\alpha < \alpha_c$). This problem can be addressed by keeping the extrusion nozzle at the last extrusion point for a few seconds while no more ink is extruded.

Figure 7(*b*) shows optical images of the microsprings fabricated at different deposition speeds (0.1–0.7 mm s^{-1}) and a constant extrusion pressure of ∼1 MPa. At a relative low deposition speed (0.1–0.2 mm s^{-1}), the extruded filament did not follow the designed path. For an accurate fabrication, the UV exposure zone should be adjusted such that the filament is exposed to the UV radiation shortly after extrusion which

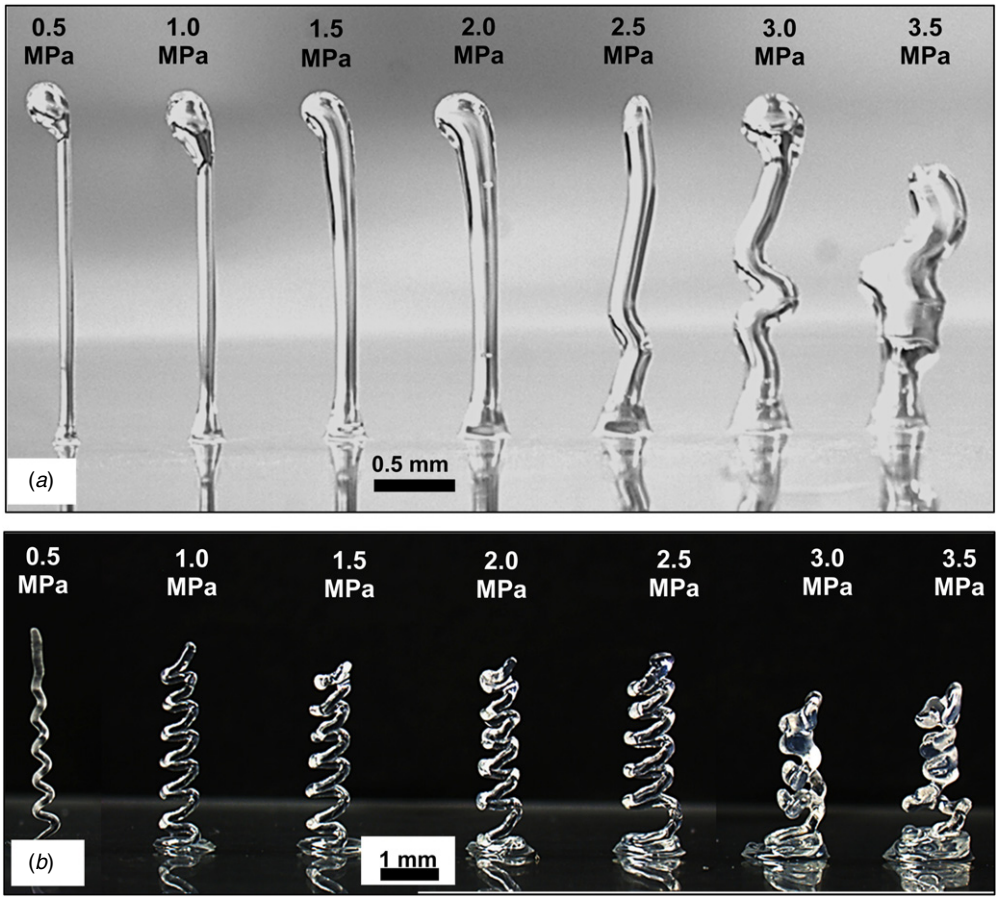

Figure 8. UV-3DP fabrication of (*a*) vertical filaments and (*b*) freeform microsprings at different extrusion pressures and a constant deposition speed of ∼0.5 mm s^{-1} using an extrusion nozzle of 150 μm-internal diameter and the UV-PU resin, NEA 123T.

allows the increase in rigidity upon curing. Therefore, at the low deposition speeds, it takes longer for the filament before reaching the exposure region (meeting the UV-light), thus the filament may slump by its weight as a result of incomplete curing. In other words, the rigidity of the extruded filaments was not high enough (i.e., $\alpha < \alpha_c$) to provide structural support for the material being deposited. In addition to incomplete curing, the possible filament bending due to the mismatch between the deposition speed (<0.4 mm s^{-1}) and the extrusion pressure/speed contribute to some extent to the unsuccessful fabrication. As the deposition speed increased (0.3–0.4 mm s^{-1}), stable filaments with geometries close to the designed path were observed. The best match was achieved at the deposition speed of 0.4 mm s^{-1} (matching the extrusion pressure/speed (∼0.4 mm s^{-1})) that enabled the accurate fabrication of microsprings composed of seven turns for a total height of 7 mm with the middle coils having a pitch of ∼1 mm. A further increase of the deposition speed (0.5–0.7 mm s^{-1}) led to the fabrication of the microcoils having smaller diameter than their programmed diameter. This issue may come from the fact that the rigidity increase of newly deposited material is not high enough due to the short UV exposure time. Therefore, the extruded filament has the same rigidity from its extrusion point to the previous support point so that the filament moves along the extrusion nozzle changing direction. To address this issue and have relatively high fabrication rates, materials with higher polymerization rates should be used. Another contribution may come from the mismatch between the deposition speed and the extrusion pressure/speed (>0.4 mm s^{-1}) that leads to the stretching and the deformation of the filament.

3.2.3. Extrusion pressure. The effect of the extrusion pressure on the UV-3DP of the structures was investigated, while keeping the deposition speed constant. Figure 8(*a*) shows optical images of the vertical lines fabricated at seven different extrusion pressures (0.5–3.5 MPa) and a constant deposition speed of ∼0.5 mm s^{-1}. The extrusion speed of the material inside the micronozzle was estimated for the seven extrusion pressures by extrapolating the apparent viscosity of the material from figure 3(*a*) and using equation (1) (see section 3.2.2). Table 1 lists the estimated extrusion speeds for the seven extrusion pressures used. The fabricated vertical filaments were straight and stable for the pressures up to 2 MPa with the increase of filaments' diameter with increasing the extrusion pressure. Above this pressure, either waved or non-shape filaments were observed, confirming the importance of well-matching the extrusion pressure/speed and the deposition speed. As listed in table 1, for the first two relatively low pressures (0.5–1 MPa), the estimated extrusion speeds were below the deposition speed (0.5 mm s^{-1}). Therefore, filament stretching is most possibly responsible for the smaller diameter of the filaments (<the

Table 1. Estimated extrusion speeds based on capillary equations for seven extrusion pressures used.

Extrusion pressure (MPa)	Extrapolated viscosity from figure 3(*a*) (Pa.s)	Estimated extrusion speed based on capillary equations (mm s^{-1})
0.5	240	0.1
1	115	0.4
1.5	100	0.6
2	80	1.2
2.5	70	1.6
3	65	2.3
3.5	60	2.9

extrusion nozzle's ID). The fabrication of the filaments at the pressures of 2.5 and 3 MPa gradually made the filaments less stable and produced buckling instability. This instability is possible due to incomplete polymerization (i.e., $\alpha < \alpha_c$) because of insufficient UV exposure time and also bending of filament as result of the deposition speed and extrusion pressure/speed mismatch (>0.5 mm s^{-1}) for the relatively high material flow rate.

Figure 8(*b*) shows optical images of the microsprings fabricated at different extrusion pressures (0.5–3.5 MPa) while maintaining a constant deposition speed of ~0.5 mm s^{-1}. The fabrication of microsprings at the lowest extrusion pressure (0.5 MPa) was unsuccessful so that either the extruded material lost their filamentary shape mostly after the first coil was fabricated or a vertical wavy filament was obtained, as can be seen in figure 8(*b*). This relatively low extrusion pressure (associated to an extrusion speed of ~0.1 mm s^{-1}) may result in a mismatch with the deposition speed which leads to stretching of the filament when the deposition speed was set at 0.5 mm s^{-1}. At the pressures above 1 MPa, more stable filaments were observed, although the fabricated microsprings featured different shapes, heights and coil diameters. At pressures of 1 and 1.5 MPa, the estimated material extrusion speeds of 0.4—0.6 mm s^{-1} (see table 1) were close to the deposition speed of 0.5 mm s^{-1}. Thus, the microsprings geometry were close to the programmed design, indicating the proper selection of the processing parameters. Similar to the microsprings fabricated at low deposition speeds (0.1–0.2 mm s^{-1}) shown in figure 7(*b*), applying relatively higher pressures (3–3.5 MPa) led to the fabrication of non-shape structures most probably due to incomplete curing of the filaments and also their possible bending caused by a mismatch between the deposition speed and the extrusion pressure/speed.

3.3. Processing map based on materials and processing criteria

The experiments shown in section 3.2 were selectively repeated for a few materials either pure resins or their nanomaterials filled nanocomposites having shear-thinning viscosity behaviors similar to those shown in figure 3. The extrusion nozzles diameter used were 100 or 150 μm. A processing map was created under those conditions for the UV-assisted 3DP technique. Figure 9 shows the processing

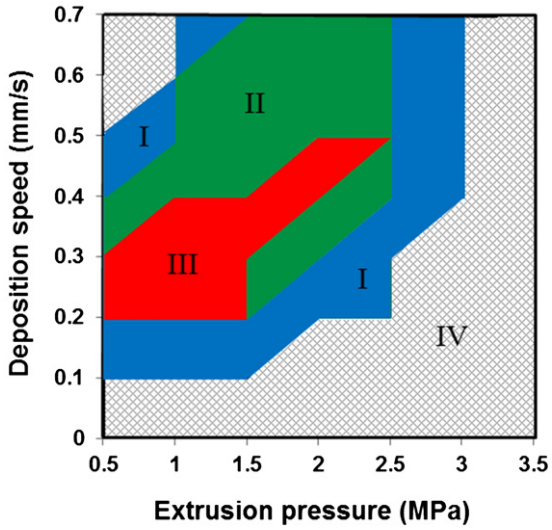

Figure 9. UV-3DP processing map for the fabrication of different microstructures at an adjusted UV intensity and exposure zone. Zone I (blue): vertical microrods, zone II (green): self-supported structures, zone III (red): 3D freeform structures, and zone IV: unsuccessful fabrication.

map drawn based on the two most important processing parameters which are the extrusion pressure and the deposition speed. The diameter of the extrusion nozzle is found to affect only the extrusion pressures so that less pressure is required for the extrusion of material through larger nozzle diameter and vice versa. The UV intensity was set for all the experiments at 50 mW cm^{-2}, match with the UV-curing kinetics of the materials. The UV-exposure zone was also adjusted such that the filament is exposed to the UV radiation slightly after extrusion and kept constant.

For successful and accurate fabrication of vertical microrods, 3D self-supported and 3D freeform microstructures, the manufacturing parameters as well as the intrinsic properties of the materials have to be properly chosen. After a material met the criteria for the viscosity and polymerization rate required for the UV-3DP technique, the extrusion pressure and the speed will be matched to achieve the critical conversion rate, α_c, which may vary depending on the desired geometry. The large area of zone I indicates that a vertical microrod can be fabricated in a broad range of pressures and speeds using different materials. Zone II which is part of zone I, shows that the range of the parameters are limited for the fabrication of self-supported or layer-by-layer microstructures when compared to those of the microrods. It indicates that a higher value of α_c is required for the fabrication of layered structures due to possible buckling of the filaments between two support points at an incomplete curing. Processing zone is much narrower for the fabrication of 3D freeform structures as shown in figure 9 in zone III. Further increase of the filament rigidity (i.e., much higher α_c) is required, which limits the range of extrusion pressures and speed. In this case, a slight mismatch between the extrusion pressure and the deposition speed affects the fabricated structure shapes which may be far from the programmed trajectory. Zone IV shows the range of parameters in which

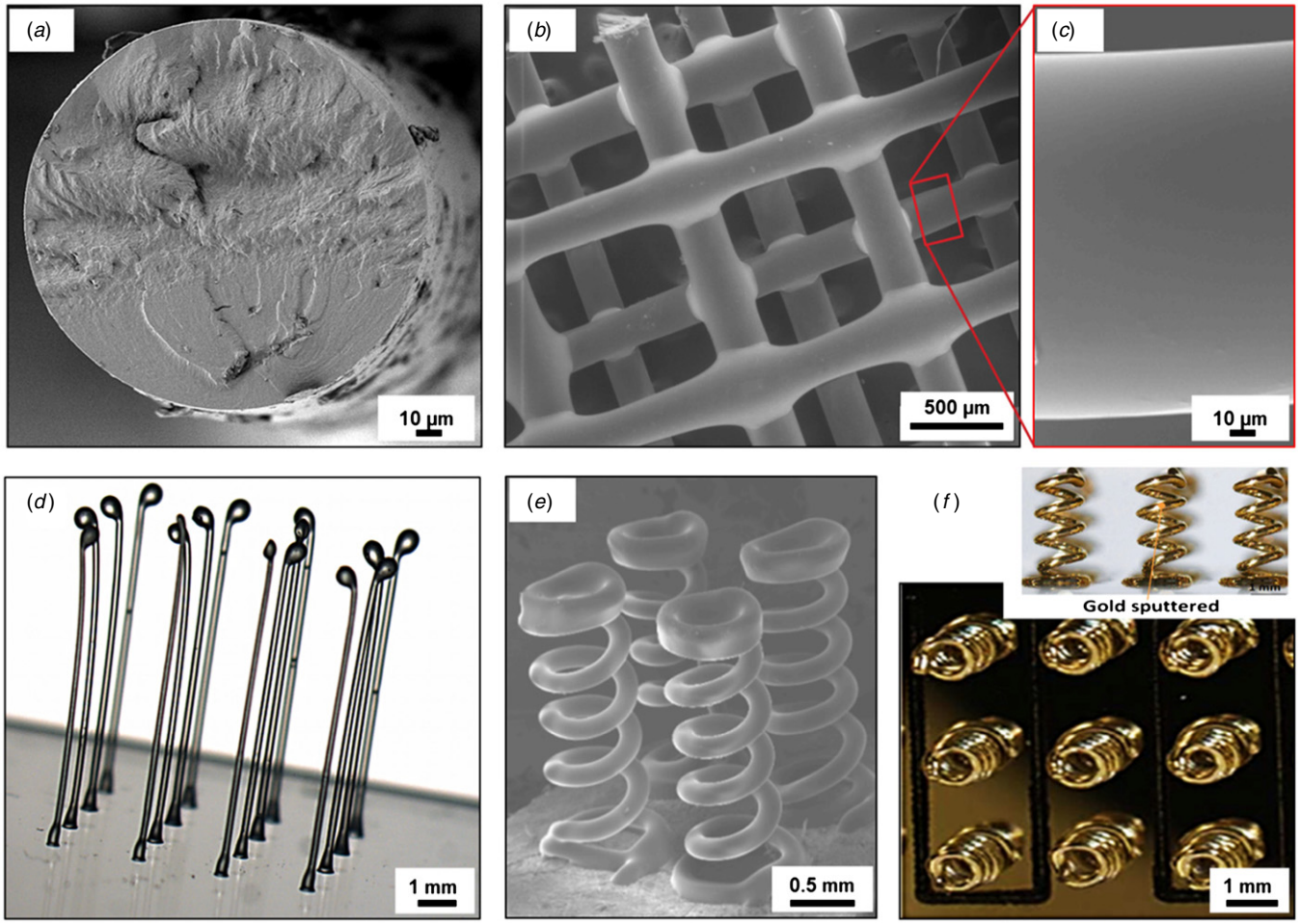

Figure 10. Optical and SEM images of several representative microstructures fabricated using the UV-3DP technique: (*a*) a typical fabricated filament cross-section, (*b*) a 3D periodic four-layer scaffold, (*c*) higher magnification of (*b*), (*d*) a network of 16 vertical microrods, (*e*) a network of four nanocomposite microsprings, (*f*) a network of nine gold-sputtered microsprings electrodes.

the UV-3DP was unsuccessful with our UV set-up and the materials used in this study. In general, the fabrication of the 3D complex structures is found to be more complicated than that of vertical microrods in which the fabricated filament is along the direction of extrusion. This allows the vertical filament to uniformly expose to the UV light, which is not the case for the 3D self-supported and freeform microstructures.

3.4. Fabrication of 3D supported and freeform structures

Various complex freeform and self-supported microstructures were fabricated, as shown in figure 10. Table 2 lists the detailed information of the manufactured microstructures such as geometry, feature size, processing conditions and type of materials used. Figure 10(*a*) shows an SEM image of a typical filament circular cross-section having a diameter of ∼120 μm. The filament spanned two rectangular pads with a distance of 10 mm and was fabricated with the UV-epoxy nanocomposite (containing 1 wt% CNTs). The fabricated very high aspect ratio (length/diameter (L/D) equals to ∼65) filament could be used as highly-sensitive nanocomposite sensor to accurately measure the strain of a structure under mechanical loadings [14]. In general, the concept of nanocomposite-based strain sensors is based on their electromechanical sensitivity that stems from the rearrangement of percolating conducting pathways (e.g., nanotubes pathway) induced by an external mechanical disturbance [15]. The freestanding feature of the filament fabricated here may lead to avoid capturing of undesired parasitic perturbations (local cracks, plasticity, etc) in applications where overall measurements are sought [14].

The flexibility of the UV-3DP methods enabled to fabricate 3D periodic scaffolds with a desired overall size, filaments length and diameter having potential applications in tissue engineering. In these applications, filament spacing (or porosity of the structure) is of great importance. Figure 10(*b*) displays the enlarged SEM image of a representative four-layer scaffold featuring 15 filaments in each layer in a square fashion, which composed of the filaments having a length of ∼15 mm and a diameter of ∼200 μm with the filament spacing of 1 mm. Figure 10(*c*) is a close-up view of the smooth surface of a filament in figure 10(*b*). Contrary to other techniques such as direct-writing of a fugitive ink filaments whose spacing in a given layer is limited to approximately ten times the filament diameter (L/D of 10) [16], the significant increase of the filament rigidity in the UV-3DP technique prevented sagging of the filaments fabricated over the underlying layer featuring a long filament spacing. Owing to this unique capability, the

Table 2. Detailed information (geometry, feature size, processing conditions and materials used) for the fabrication of microstructures shown in figure 10.

Figure 10	Geometry and feature size	Materials used	Nozzle ID (μm)	Extrusion pressure (MPa)	Deposition speed (mm s^{-1})
(a)	A single filament having 10 mm length	UV-epoxy nanocomposites (1 wt% CNTs)	100	~1.5	0.4
(b, c)	four-layers scaffold with filament span of 1 mm	UV-PU (NEA 123T)	150	~1.5	0.3
(d)	A network of 16 vertical rods (L/D:100)	UV-PU (NEA 123T)	150	~1	0.6
(e)	A network of four microsprings	UV-epoxy nanocomposites (1 wt% CNTs)	100	~1.5	0.2
(f)	A network of 15 gold-sputtered microsprings	UV-PU (NEA 123T)	150	~1	0.4

spacing between filaments (i.e., structural porosity) in a given layer could be easily tailored in order to provide an appropriate condition, in term of structural-dependent parameters, for cell attachment and growth [17].

Figure 10(*d*) shows an optical image of a microrods network composed of 16 identical vertical microrods having a length of ~15 mm and a diameter of ~150 μm (L/D of ~100). The network was fabricated in a square layout (4 × 4) having a rod spacing of 3 mm. This type of microdevice might find applications in MEMS and lab-on-a-chip systems, for instance, as surface enhancement textures in gas and biosensors and in solar cells [18]. In the literature, a rod aspect ratio of up to 50 has been achieved using photolithography techniques in order to make such a device to entrap kidney cells. A network consisting of hundreds of microrods featuring considerably larger aspect ratio of up to few hundreds can be manufactured using the UV-3DP technique.

Figure 10(*e*) shows an SEM image of network of microsprings made of carbon nanotube-based nanocomposite materials with potential MEMS application such as freeform strain sensor with a possible capability of sensing out-of-plane strains [15]. This nanocomposite-based microdevice consists of four identical freeform microsprings with seven 1 mm diameter coils and inter-coil distance of 3 mm. The height of microsprings was ~6 mm and the filament's diameter was ~150 μm. Figure 10(*f*) shows optical images of a fabricated network which is composed of 9 gold-sputtered 3D freeform microsprings with high potentials in lab-on-a-chips. This manufactured interdigitated 3D microelectrode might be used to build a real lab-on-a-chip device in order to promote cell separation (e.g., cancer cell detection) through dielectrophoresis forces, representing higher efficiency when compared to standard planar microelectrodes [19]. The flexibility of the UV-3DP technique enables the accurate fabrication of complex 3D microstructures with different geometries for various technological applications such as MEMS, microelectronics, and tissue engineering.

4. Conclusion

In the present work, the effects of manufacturing conditions of the UV-3DP technique were thoroughly investigated in order to find a processing map for successful and accurate freeform fabrication of 3D self-supported and freeform structures. It was found that for successful and accurate fabrication of 3D structures, the deposition speed, the pressure applied to the material, and the UV-radiation intensity have to be adjusted according to the viscosity and the curing rate of the extruded material. Once the proper condition was applied, the manufactured microstructures geometry matched the programmed robot's paths and the fabrication was reproducible. A higher increase of the filament rigidity was required for the fabrication of freeform microstructures, which limited the processing condition to a much narrower zone, when compared to that of self-supported structures. The detailed results presented in this study may help understand better the parameters influencing the UV-3D printing of microstructures with various geometries and may offer a general overview of the technique with its capabilities. Further studies should focus on the creation of a dimensionless processing map to extend its applicability. This next step will require taking into account the material's photopolymerization kinetics during the fabrication of a structure.

Acknowledgments

The authors acknowledge the financial support from FQRNT (Le Fonds Québécois de la Recherche sur la Nature et les Technologies). The authors would like to thank Professor Martin Levesque from Ecole Polytechnique de Montreal for the technical advice.

References

[1] Thostenson E T and Chou T-W 2006 Carbon nanotube networks: sensing of distributed strain and damage for life prediction and self healing *Adv. Mater.* **18** 2837–41
[2] Sandler J K W, Kirk J E, Kinloch I A, Shaffer M S P and Windle A H 2003 Ultra-low electrical percolation threshold in carbon-nanotube-epoxy composites *Polymer* **44** 5893–9
[3] Tsai Y C, Li S C and Chen J M 2005 Electrochemical sensors based on multi-walled carbon nanotube-nafionTM nanocomposite film for determination of heavy metals and hydrogen peroxide *Proc. 5th IEEE Conf. on Nanotechnology (Nagoya, Japan)* pp 642–5
[4] Sahoo N G, Jung Y C, Yoo H J and Cho J W 2007 Influence of carbon nanotubes and polypyrrole on the thermal, mechanical and electroactive shape-memory properties of polyurethane nanocomposites *Compos. Sci. Technol.* **67** 1920–9
[5] Halary J, Cookson P, Stanford J L, Lovell P A and Young R J 2004 Smart nanostructured polymeric coating for use as remote optical strain sensors *Adv. Eng. Mater.* **6** 729
[6] Liska R *et al* 2007 *J. Coat. Technol. Res.* **4** 505
[7] Kawata S, Sun H B, Tanaka T and Takada K 2001 Finer features for functional microdevices *Nature* **412** 6848

[8] Lebel L L, Aissa B, El Khakani M A and Therriault D 2010 Ultraviolet-assisted direct-write fabrication of carbon nanotube/polymer nanocomposite microcoils *Adv. Mater.* **22** 592

[9] Le Borgne V, Aissa B, Mohamedi M, Kim Y A, Endo M and El Khakani M A 2011 Pulsed KrF-laser synthesis of single-wall-carbon-nanotubes: effects of catalyst content and furnace temperature on their nanostructure and photoluminescence properties *J. Nanoparticle Res.* **13** 5759

[10] Farahani R D, Dalir H, Le Borgne V, Gautier L A, El Khakani M A, Lévesque M and Therriault D 2012 Reinforcing epoxy nanocomposites with functionalized carbon nanotubes via biotin–streptavidin interactions *Compos. Sci. Technol.* **72** 12

[11] Zein I, Hutmacher D W, Tan K C and Teoh S H 2002 Fused deposition modeling of novel scaffold architectures for tissue engineering applications *Biomaterials* **23** 1169

[12] Bruneaux J, Therriault D and Heuzey M C 2008 Micro-extrusion of organic inks for direct-write assembly *J. Micromech. Microeng.* **18** 115020

[13] Lebel L L, Aissa B, El Khakani M A and Therriault D 2010 Preparation and mechanical characterization of laser ablated single-walled carbon-nanotubes/polyurethane nanocomposite microbeams *Compos. Sci. Technol.* **70** 3

[14] Farahani R D, Dalir H, Le Borgne V, Gautier L A, El Khakani M A, Lévesque M and Therriault D 2012 Direct-write fabrication of freestanding nanocomposite strain sensors *Nanotechnology* **23** 8

[15] Hu N, Karube Y, Yan C, Masuda Z and Fukunaga H 2008 Tunneling effect in a polymer/carbon nanotube nanocomposite strain sensor *Acta Mater.* **56** 13

[16] Therriault D, White S R and Lewis J A 2003 Chaotic mixing in three-dimensional microvascular networks fabricated by direct-write assembly *Nature Mater.* **2** 265

[17] Kan Wang L C, Zhang L, Dong J and Wang S 2012 Biodegradable photo-crosslinked polymer substrates with concentric microgrooves for regulating MC3T3-E1 cell behavior *Adv. Healthc. Mater.* **1** 10

[18] Yoo J S, Kim K, Thamilselvan M, Lakshminarayn N, KimY K and Lee J 2008 RIE texturing optimization for thin c-Si solar cells in SF_6/O_2 plasma *J. Appl. Phys.* D **41** 125205

[19] Khoshmanesh K, Zhang C, Tovar-Lopez F J, Nahavandi S, Baratchi S, Mitchel A and Kalantar-Zadeh K 2010 Dielectrophoretic-activated cell sorter based on curved microelectrodes *Microfluidics Nanofluidics* **9** 411